THE ASTROPHYSICAL JOURNAL, 265:26–34, 1983 February 1

THE X-RAY MORPHOLOGY OF ABELL 1367

J. BECHTOLD,[1] W. FORMAN, R. GIACCONI,[2] C. JONES, J. SCHWARZ,
W. TUCKER,[3] AND L. VAN SPEYBROECK
Harvard-Smithsonian Center for Astrophysics
Received 1981 July 24; accepted 1982 July 30

ABSTRACT

X-ray observations of the nearby cluster Abell 1367 were made with the Imaging Proportional Counter (IPC) and High Resolution Imager (HRI) aboard the *Einstein Observatory*. We used the IPC to study the diffuse cluster emission. With the HRI we detected eight point sources above the diffuse cluster emission, three of which are apparently associated with cluster galaxies. In addition, the HRI observations have resolved 13 extended features with characteristic radii of order 1′, eight of which are associated with cluster galaxies. These extended sources have luminosities of $1.5–6.5 \times 10^{41}(H_0/50)^{-2}$ ergs s^{-1} in the 0.5–4.5 keV band and constitute about 6.0% of the total cluster emission. We discuss how these hot galactic coronae can be maintained.

Subject headings: galaxies: clusters of — galaxies: structure — X-rays: sources

I. INTRODUCTION

Although 10 years have elapsed since clusters of galaxies were discovered to be X-ray emitters (Gursky *et al.* 1971; Kellogg *et al.* 1972; Forman *et al.* 1972), it has been only with the advent of an X-ray imaging observatory that a detailed study of cluster X-ray morphology has become possible. Jones *et al.* (1979) studied the first *Einstein Observatory* cluster results and concluded that cluster X-ray morphology closely correlates with the degree of dynamical relaxation as determined by the morphology of the galaxy distribution, the velocity dispersion, X-ray luminosity, and X-ray gas temperature. In particular, they found that unrelaxed, young clusters such as Virgo and Abell 1367 have X-ray emission that is clumpy, usually enhanced around member galaxies. Relaxed clusters, on the other hand, were found to show smooth X-ray emission associated with the cluster as a whole, though often centered and peaked about a single central dominant galaxy (e.g., Abell 85).

In this paper, we attempt to place the qualitative description of Jones *et al.* on a quantitative foundation. For A1367 we establish the statistical significance of both point and small-scale extended features superposed on the large-scale cluster component. X-ray observations of the Coma Cluster (Ku 1981) and a Deep Survey field in Cetus (H7533) have been used to verify our analysis procedures.

[1] And Steward Observatory, University of Arizona.
[2] And Space Telescope Science Institute.
[3] And University of California, Irvine.

II. OBSERVATIONS

The Imaging Proportional Counter (IPC) and High Resolution Imager (HRI) on the *Einstein Observatory* are described by Giacconi *et al.* (1979*a*). The observations of Abell 1367 performed with the IPC and HRI extend those presented by Jones *et al.* (1979) and are summarized in Table 1.

Our analysis covers four topics: (*a*) location and identification of point sources; (*b*) determination of the noncluster background; (*c*) identification of extended emission on scales small compared to the cluster; and (*d*) study of the diffuse cluster emission.

a) Point Sources

Since the cluster emission causes the X-ray surface brightness to vary over the field of view, the source detection technique described by Giacconi *et al.* (1979*b*)

TABLE 1

SUMMARY OF OBSERVATIONS

Sequence No.	Year/Day	Target Coordinates	Instrument	Exposure Time (s)
296a	78/352	$11^h41^m54^s.00$, 20° 7′ 0″.00	IPC	6351
296b	79/352–3	11 41 54.00, 20 7 0.00	IPC	20,738
6062	79/359–60	11 42 0.00, 20 8 0.00	HRI	37,761
6333	79/360	11 42 17.00, 19 57 56.9	HRI	17,746
8952	80/156–174	11 41 20.00, 20 13 0.00	HRI	9303

was modified. Instead of using counts summed over the entire field to compute the background, we calculated the background locally over a smaller region adjacent to the candidate source location.

This local detection algorithm was used to find point sources in the HRI fields individually, and in their sums where they overlap, with sliding detection cells of size 12″ × 12″, 24″ × 24″, and 36″ × 36″. The point response function is broadened by the coma of the telescope, and so the optical cell size for point source detection varies across the field of view. For each cell size, the background was measured in a square with linear size 3 times the linear size of the detection cell. The adopted source threshold was 3.5 σ in flux, which, when applied to the Cetus Deep Survey field, H7533, resulted in the detection of only those sources previously detected using the standard detection routines and thresholds (Giacconi *et al.* 1979*a*, *b*). This threshold in flux is equivalent to the requirement that the number of spurious sources per field due to random fluctuations be less than 1, or that the probability that a source at the threshold is spurious be less than 10^{-6}. Table 2 gives the results for this point source analysis of A1367, and lists positions and uncertainties, detection cell sizes, net counts above background, counts per second, and optical candidates. Figure 1 (Plate 1) gives finding charts for all sources except 3C 264, which was discussed by Elvis *et al.* (1981).

These point sources (Table 2) are typical of those found in Deep Surveys both in total number and in type of optical counterpart with the exception of the three galaxies which are associated with A1367 (Giacconi *et al.* 1979*b*; Griffiths *et al.* 1982). At the distance of A1367 ($z = 0.0214$) the luminosities of these three galaxies range from 4×10^{40} to $2.4 \times 10^{42}(H_0/50)^{-2}$ ergs s^{-1}.

b) Noncluster Background

We obtained the HRI background due to particles, detector noise, and diffuse X-rays by measuring the flux in the NE region of field 6062 that has a minimum counting rate. This flux is 0.00439 ± 0.00005 counts arcmin^{-2} s^{-1} and represents an upper limit to the noncluster background. Attempts to use a background determined from Deep Survey fields were unsuccessful, because of the differing particle environments intersected by the shifting orbital plane of the satellite. If the diffuse cluster emission extends to the minimum flux region, the true noncluster background would, of course, be lower. Field 6062 shows an overall excess of 0.5 counts s^{-1} above this background, corresponding to a luminosity of $6.1 \times 10^{43}(H_0/50)^{-2}$ ergs s^{-1}, in the 0.5–4.5 keV energy band which is comparable to the cluster luminosity measured with the IPC. The luminosity determined using the HRI is uncertain by about 30% due to the uncertainty in the source

TABLE 2

HRI Point Sources

α(1950.0) δ(1950.0)	Field	Cell Size	Positions Error Radius	Net Counts above *b*	Counts s^{-1} ($\times 10^{-4}$)	Optical Candidate
11^{h}41^{m}21^s.8 20°13′ 31″.9	6062	12″	11″	55 ± 8	14.6 ± 2.0	Blue object
11 41 30.4 20 14 15.9	NM	24″	14″	27 ± 8	4.9 ± 1.4	Blue object
11 42 16.8 20 01 03.6	SM	12″	11″	19 ± 5	3.4 ± 0.9	No obvious counterpart
11 42 17.3 20 08 19.3	6062	12″	11″	20 ± 5	5.3 ± 1.3	No obvious counterpart
11 42 22.0 20 00 10.9	SM	12″	11″	20 ± 6	3.6 ± 1.1	Galaxy 41
11 42 22.6 20 04 39.5	SM	12″	11″	19 ± 5	3.4 ± 0.9	No obvious counterpart
11 42 26.4 20 02 36.1	6062	12″	11″	30 ± 7	7.9 ± 1.9	Galaxy 52
11 42 29.9 19 53 06.4	6333	12″	10″	287 ± 17	15.7 ± 0.9	3C 264 = NGC 3862

Note.—SM = south merge, i.e., overlap region of fields 6333 and 6062.
NM = north merge, i.e., overlap region of fields 6062 and 8952.

spectrum, and amount of absorption by hydrogen in our Galaxy.

c) *Clumpy X-Ray Emission*

To search for emission from extended sources of characteristic lengths small compared to the cluster, the local detection algorithm was repeated for larger detection cell sizes, 24″, 36″, 1′, 1.′5, and 2′. The identical analysis was performed for the Deep Survey field in Cetus, and a threshold for detection of 3 σ above background was chosen. Results for the A1367 field 6062 and Cetus are shown in Table 3, for these detection cells. In initially establishing a characteristic scale size, we restricted our analysis to an area in the center of the 6062 field of view which excluded the strong point sources associated with 3C 264 to the southeast and the blue object to the northwest, and a region of equal area in Cetus. It is clear from Table 3 that a number of sources appear in the A1367 field on scales larger than 36″ and smaller than 2′. Not tabulated are previously detected point sources associated with background objects. Some extended sources are detected in more than one bin size and are included each time. The maximum at 1′ establishes a characteristic angular scale which appears to be a property of sources in A1367, since no such effect is observed in Cetus. The probability of detecting nine sources due to random fluctuations when we expect one is 1.1×10^{-7}. The single 1′ detection in Cetus is an extended source associated with a poor group of galaxies.

To show that these sources are not an artifact of the local detection algorithm when applied to a nonflat background, we repeated these procedures on the *Einstein* HRI observations of the Coma Cluster (Ku 1981). We detected a single 1′ source in Coma which coincides with the cluster center and is due to the limitations of our detection algorithm which cannot properly evaluate background in the peak region. For Coma, this detection represents a negligible fraction (0.1%) of the total diffuse cluster luminosity. However, if point and extended sources with luminosities like those found in A1367 existed in Coma, the higher level of general cluster emission would make them undetectable with the present observations. Three sigma upper limits for the luminosities of the Coma galaxies, each measured in a circle of area 1 arcmin^2 are $(4.5\text{–}5.0) \times 10^{42}(H_0/50)^{-2}$ ergs s^{-1}, well above the luminosities of detected 1′ sources in A1367.

To further study the 1′ features in A1367 the HRI images were smoothed with a Gaussian of sigma 16″. From this smoothed map, we have subtracted a second map, this one smoothed with a Gaussian function 3′. The resulting difference map retains the small-scale extended features, but eliminates the large-scale cluster emission. Figure 2 (Plates 2 and 3) displays these "iso-sigma" contours for the A1367 1′ sources. Figure 3 (Plate 4) shows the contours of the entire central field.

TABLE 3

HRI Source Detection with Varying Cell Size

Field	24″ $>3.5\,\sigma$	36″ $>3.5\,\sigma$	1′ $>3\,\sigma$	1.′5 $>3\,\sigma$	2.′0 $>3\,\sigma$
A1367(6062)	2	3	9	3	2
Cetus	3	3	1	0	0
Coma	1	1	1	0	0

We applied the local detect algorithm to the three HRI fields in A1367, and their merged overlapping regions. Estimates for the luminosities of the 1′ sources can be made by using their detected intensities. However, since in the local sliding bin detection algorithm we assume that a source has a square shape, errors are introduced by variations in source morphology. Therefore, we accounted for the source irregularity by subsuming in the source luminosity all counts enclosed by a single isointensity contour. The background was taken from the area outside the 1 σ contour and within a circle of area 9 arcmin^2 centered on each source. This background was subtracted from the summed counts within the 1 σ contour to yield the intensity. Table 4 lists the source positions, areas, net counts, luminosities, and optical candidates. The luminosities are uncertain by 30% as a result of uncertainties in the source spectrum and galactic absorption.

Using a magnitude-limited sample of galaxies ($m_J \leq 17.0$) selected by Oemler (1980), we find there is an association of these sources with cluster galaxies. In the central area of field 6062, the 1′ detected sources occupy 4.3% of the area and include seven of Oemler's galaxies within their 1 σ contours. This region contains 19 galaxies in Oemler's list. Given random uncorrelated distributions of sources and galaxies, the probability that seven of the 19 galaxies will be contained within source contours is less than 10^{-5}. If the galaxies are not randomly distributed, but are grouped into subcondensations, we may have underestimated the probability that the galaxy–1′ source associations are spurious. In this case, a particular 1′ source may mark the peak of slightly more extended emission associated with a clump of galaxies, and not be associated with a specific galaxy in the clump. We have looked for evidence of clumping of the galaxies in our sample by comparing the difference in velocity between a galaxy and its nearest neighbor with the difference in velocity of the galaxy and the cluster mean velocity. Although Oemler's galaxy counts show subclustering on larger scales, we found that there was no evidence for subcondensations on small scales (3–4 galaxies) in our sample, so that subclumping is not affecting the probability of spurious galaxy–1′ associations computed above. We conclude that there is a significant association of 1′ sources with cluster galaxies. There are, however, four sources with no such association. One source (No. 2) appears associated with a background group of galaxies, two others may be associated with faint objects, and the fourth has no candidate objects to an apparent magnitude $m_R < 22$ (see Fig. 2).

Table 5 lists optical and radio data for the galaxies surveyed, and upper limits to the X-ray emission from the

TABLE 4

HRI EXTENDED SOURCES

α(1950.0) δ(1950.0)	Field	Area (arcmin²)	Net Counts	Counts s⁻¹	L_x	Optical Candidates
11h41m27s.7 20°03′ 42″.8	6062	1.64	160.6 ± 21.9	4.3×10^{-3}	6.2×10^{41}	galaxy 18
11 41 33.9 20 07 03.7	6062	2.02	92.0 ± 24.3	2.4×10^{-3}	...	background cluster
11 41 37.3 20 04 42.9	6062	0.85	57.9 ± 15.1	1.5×10^{-3}	...	no candidates
11 41 42.0 20 06 48.8	6062	0.78	39.0 ± 14.1	1.0×10^{-3}	1.5×10^{41}	galaxy 23
11 41 51.8 20 00 27.2	6062	1.21	95.5 ± 19.0	2.5×10^{-3}	3.7×10^{41}	galaxy 27
11 42 01.6 20 08 20.0	6062	1.42	82.6 ± 19.4	2.2×10^{-3}	...	several faint objects
11 42 10.2 20 02 05.5	6062	2.06	118.5 ± 25.0	3.1×10^{-3}	4.6×10^{41}	galaxy 30
11 42 13.0 20 04 42.6	6062	1.28	73.6 ± 18.7	1.9×10^{-3}	2.9×10^{41}	galaxy 35
11 42 12.8 19 58 15.0	6062	3.13	168.7 ± 32.6	4.5×10^{-3}	6.5×10^{41}	galaxy 33 and/or galaxy 29
11 41 08.3 20 22 11.7	8952	2.77	63.1 ± 14.6	6.78×10^{-3}	...	faint object
11 41 44.1 20 15 43.9	NM	1.07	53.2 ± 17.6	1.13×10^{-3}	1.7×10^{41}	galaxy 25
11 41 29.2 20 17 34.4	8952	1.35	39.3 ± 10.7	4.2×10^{-3}	...	no candidates
11 42 01.0 20 01 22.2	SM	1.78	139.8 ± 25.8	2.52×10^{-3}	3.7×10^{41}	galaxy 53
11 42 23.5 20 10 49.7	6062	see n. 3	9.5 ± 2.7	...	...	fuzzy faint object
11 41 48.1 20 03 09.9	6062	see n. 4	89.4	2.4×10^{-3}	3.5×10^{41}	galaxy 55

NOTES.—(1) NM = north merge, i.e., overlap region of fields 8952 and 6062.
(2) SM = south merge, i.e., overlap region of fields 6333 and 6062.
(3) Detected only in 36″ × 36″ bin size.
(4) Detected only in 1′.5 × 1′.5 bin size.

galaxies of Oemler's sample which were not detected above 3 σ. Galaxies that were detected above 3 σ, but were not in Oemler's list, are also included. The positions given were measured from the Palomar Sky Survey print and are accurate to 5″.

d) Diffuse Cluster Emission: IPC Results

We found that the A1367 sources detected in the HRI image are often confused in the IPC observations. The IPC has coarser resolution and requires an optimum detection cell size for point sources of 2′.4 on a side, comparable to the separations of the extended HRI sources. A further complication is that the region used to calculate the local background, perimeter of a square with 7′.2 side, samples a considerable gradient of cluster surface brightness. Therefore, the IPC data were used primarily to study the diffuse emission, although the contour map in Figure 4 (Plate 5) shows that the emission is not smooth on small scales.

To estimate the IPC background, we used the average value measured in over 100 other fields, 1.2×10^{-4} counts s^{-1} $arcmin^{-2}$ keV^{-1} with an uncertainty of 12% due to variations among the fields. With this background subtracted, the 0.5–3.0 keV flux within 0.5 Mpc of the cluster center is 0.96 ± 0.03 counts s^{-1} corresponding to $4.5 \times 10^{43}(H_0/50)^{-2}$ ergs s^{-1}, adopting a thermal bremsstrahlung spectrum with $kT = 2.8$ keV (Mushotzky *et al.* 1978). The uncertainty in the luminosity is dominated by systematic uncertainties in the detector calibration and is accurate to 15%. Assuming an isothermal sphere model, we calculated core radii of 0.80 Mpc and 0.42 Mpc along the long and short axes, respectively, of the cluster emission. The position angle (angle of major axis from north toward east) of the X-ray emission is 135° ± 7°. Carter and Metcalf (1980) with a deep ($m < 20$) galaxy sample have measured an ellipticity of 0.50 ± 0.10 and position angle of 121° ± 7° for the inner 1 Mpc of A1367, in good agreement with our X-ray results.

III. DISCUSSION

Observations indicate that Abell 1367 is a young, dynamically unevolved cluster. Its irregular appearance and low central concentration, both optically (Carter and Metcalf 1980; Bahcall 1977) and in X-rays suggest that it has not fully relaxed. In the absence of dissipation,

TABLE 5

GALAXIES IN A1367 HRI FIELDS

No.	α(1950.0) δ(1950.0)	Field	Zwicky or NGC Number	L_x[a] (10^{41} ergs s^{-1})	Type[b]	m_J[c]	Radial Velocity (km s^{-1})	H I log $M_\odot$	Comments
1	$11^h40^m20^s.78$ 20°14′ 35″.6	8952	97-073	<9.3	Sc pec Sc[d]	15.9	7239[e]	9.09[n]	Hα[f]
2	11 41 29.91 20 16 26.7	NM	97-100 N3845	<1.1	S0	14.8	5569	...	
3	11 40 30.70 20 13 01.1	8952	S-3[g]	<4.2	S0 E[g]	16.2	...	...	
4	11 40 35.14 20 18 17.1	8952	...	<3.7	E[g]	16.9	...	...	
5	11 40 37.65 20 16 56.4	8952	97-079	<3.7	Sc pec I[d]	15.9	6942	No[d]	Hα[f]
6	11 41 00.99 20 16 12.5	8952	...	<3.7	E	16.5	...	...	
7	11 41 11.04 20 19 01.2	8952	97-086	<4.0	S0	15.9	6378	...	
8	11 41 13.53 20 14 45.7	8952	97-087 U6697	<4.9	Sp Sc[d]	14.0	6571	9.56[e]	Hα[f] Head-tail radio galaxy[h]
9	11 41 17.93 20 01 02.8	6062	...	<1.6	Sc	15.8	...	...	
10	11 41 20.86 20 10 21.9	8952	97-089 N3837	<4.0	E E[g]	13.8	6216	...	
11	11 41 21.82 20 12 48.7	8952	...	<3.7	S0	16.7	...	...	
12	11 41 22.00 20 13 53.5	8952	97-090	<4.7	S0	15.3	5969	...	
13	11 41 23.43 20 21 19.5	8952	97-091 N3840	<4.3	Sb Sb[d]	14.4	7312	9.24[e]	Hα[f]
14	11 41 23.90 20 03 24.7	6062	97-088	<1.6	S0 Ab/S0[d]	15.4	5552	...	
15	11 41 25.23 20 18 26.6	8952	97-105	<3.9	Sp ABb[d]	14.8	5368	...	
16	11 41 26.54 20 13 42.1	NM	97-095 N3842	<1.7	E E[d]	12.7	6164	...	Wide-angle tail radio galaxy[h,i]
17	11 41 26.63 20 14 59.3	8952	97-096	<3.9	E	14.8	6145	...	
18	11 41 26.29 20 03 45.2	6062	97-093	See Table 4	S0 Sbp[d]	15.8	4865	8.77[n]	Hα[f,i]
19	11 41 27.32 20 01 05.3	6062	S-17[g]	<1.6	Sc	15.8	...	...	[i]
20	11 41 28.07 20 22 37.1	8952	...	<4.4	S0 E	16.9	7933	...	
21	11 41 27.52 20 04 45.6	NM	97-094	<1.4	S0	16.1	7933	...	[i]
22	11 41 32.01 20 00 56.6	6067	97-099	<1.7	E E[g]	17.4	7661	...	[i]
23	11 41 43.51 20 07 23.2	6062	97-101	See Table 4	S0/a ABb[d]	14.5	6382	...	[i]
24	11 41 45.15 20 06 15.0	6062	97-105	<1.6	S0/a ABb	15.1	5368	...	[i]
25	11 41 44.71 20 15 31.3	NM	97-106 N3851	See Table 4	E E[g]	15.2	6398	...	
26	11 41 49.47 20 06 22.0	6062	97-110	<1.6	S0	15.5	4456	...	[i]
27	11 41 52.71 20 00 47.6	SM	97-109	See Table 4	S0 E[g]	15.9	6751	...	[i]
28	11 41 54.96 20 21 15.0	8952	97-111	<4.4	S0	14.9	NW 7020[j] SE 7363[j]	...	Probably a true double
29	11 42 09.96 19 58 30.4	SM	...	See Table 4	Sc	16.7	24,428[k]	...	[i]
30	11 42 11.02 20 02 08.4	SM	97-113	See Table 4	S0	16.3	6348	...	[i]
31	11 42 11.85 20 09 16.4	6062	97-115	<1.8	S0	15.6	7721	...	[i]
32	11 42 12.58 19 51 32.6	6333	S-24[g]	<2.9	E E[g]	16.5	...	...	

TABLE 5—*Continued*

No.	α(1950.0) δ(1950.0)	Field	Zwicky or NGC Number	L_x[a] (10^{41} ergs s^{-1})	Type[b]	m_J[c]	Radial Velocity (km s^{-1})	H I log $M_\odot$	Comments
33	11 42 12.34 19 57 58.5	SM	97-119	See Table 4	Sa Ab[d]	15.6	4869[k]	8.60[d]	[i]
34	11 42 12.19 20 03 05.9	SM	97-114	<1.5	Sc Scp[d]	15.9	8456	No[d]	"Blue and peculiar"[i]
35	11 42 13.70 20 04 24.1	SM	97-120 N3860	See Table 4	Sa Ab[d]	13.8	5390	8.47[l]	Hα[f,i]
36	11 42 13.37 20 05 10.0	SM	...	<1.5	Sc	...	20,327[k]	...	[i]
37	11 42 14.56 19 48 38.1	6333	97-117 N3857	<3.1	Sa Ab[d] E[g]	14.7	6183	No[d]	
38	11 42 16.58 19 53 16.20	6333	97-118	<2.9	S0 E[g]	16.1	6484	...	
39	11 42 19.36 20 03 17.0	SM	97-125	<1.5	Sc Sbp[d]	15.4	8177	No[d]	"Blue and peculiar"[i]
40	11 42 20.27 19 46 18.0	6333	97-123	<2.8	S0	16.2	6385	...	
41	11 42 21.45 20 00 35.5	SM	97-124	See Table 2	S0?[g] S0	16.4	S7751[k] N5962	...	Probably not a physical pair[i]
42	11 42 28.33 19 53 55.9	SM	97-128	<1.4	E	14.9	6273	...	
43	11 42 29.20 19 57 37.0	6333	S-27[g]	<3.1	E E[g]	...	...	...	
44	11 42 30.27 20 04 14.3	SM	...	<1.4	Spec	16.7	...	...	[i]
45	11 42 28.46 20 15 04.8	6062	97-129 N3861	<1.6	SB Sc[d]	13.2	4956	9.84[e]	Hα[f]
46	11 42 31.33 20 14 41.6	6062	...	<1.6	...	...	...	...	
47	11 42 33.73 19 49 56.3	6333	...	<2.6	S0	16.3	...	...	
48	11 42 35.07 19 48 41.0	6333	...	<2.6	S0	16.5	...	...	
49	11 42 38.23 20 02 03.0	6333	...	<2.7	Spec	16.7	...	...	
50	11 42 39.39 20 07 24.6	6062	97-131	<1.8	S0 E[g]	16.8	7575	...	
51	11 43 05.65 20 02 53.9	6333	S-37[g]	<2.7	E E/S0[g]	...	...	...	
52	11 42 26.22 20 02 30.5	6062	S-26[g]	See Table 2	E[g]	...	8299[k]	...	
53	11 42 00.95 20 01 46.2	SM	S-23[g]	See Table 4	E[g]	...	5766[k]	...	
54	11 42 29.56 19 53 04.3	...	N3862	79	E	...	...	...	[m]
55	11 41 46.60 20 03 06.8	6062	S-20[g]	See Table 4	E[g]	17.1	...	...	

[a] Upper limits within circle of area 1′.
[b] Galaxy types from A. Oemler (1981) except where noted.
[c] Apparent *J* magnitudes from A. Oemler 1981, except where noted.
[d] J. Stauffer 1981, private communication.
[e] G. Bothun 1981, private communication.
[f] Tifft 1978.
[g] Strom and Strom 1978*b*.
[h] Gavazzi 1978.
[i] Galaxies in complete sample.
[j] Tifft 1981, unpublished provisional redshifts subject to small (100 km s^{-1}) systematic corrections.
[k] Bechtold *et al.* 1983.
[l] Chincarini *et al.* 1982, preprint.
[m] See Elvis *et al.* 1981 for details.
[n] G. Chincarini 1981, private communication.

irregularities in the galaxy distribution will be erased by collisions, mergers, and tidal effects in about a crossing time, as will irregularities in the X-ray gas distribution (White 1976; Rees and Ostriker 1977). We stress that A1367 is irregular on scales larger than the 1′ sources (see Fig. 4) and that its irregular appearance is not due to the relative importance of individual galaxy potentials compared to the shallow cluster potential. A1367's low X-ray temperature, 2.8 ± 1.0 keV (Mushotzky *et al.* 1978), also implies a weak cluster potential, characteristic of a system in an early stage of collapse. Strom and Strom (1978*a*, *b*) found that elliptical galaxies in A1367 had characteristic sizes about 1.5 times larger than ellipticals in the cores of Coma and Perseus. They suggested that the galaxies in A1367 had undergone fewer tidal encounters with neighboring galaxies than their counterparts in Coma and Perseus and therefore could be 50% more massive. Supporting this view are 21 cm observations (Sullivan and Johnson 1978) which show that spirals in A1367, though H I deficient with respect to the field, are less H I deficient than spirals in Coma.

a) Nature of the Coronae

The extended sources around A1367 galaxies are probably hot coronae of gas and not unresolved emission from galactic point sources, since the luminosities and extents of the A1367 sources are larger than those found in the discrete source component in normal galaxies. Long and Van Speybroeck (1982) measure L_X/L_V in the range 2×10^{-4}–4×10^{-3} for a sample of 70 normal field galaxies, whereas L_X/L_V ranges from 4×10^{-3} to 4×10^{-2} for the A1367 galaxies. The extended nature of the sources also demonstrates that the X-ray emission is not associated with active galactic nuclei. We note that without the spatial resolution of the HRI, these X-ray emitting galaxies might have been misclassified as active galactic nuclei.

b) Gas Parameters

In Table 6 we list parameters describing the physical conditions in the components of the X-ray emitting gas in A1367. In deriving the cluster gas density, we used the emissivity calculations of Raymond, Cox, and Smith (1976) and assumed that the large-scale structure is represented by an isothermal gas sphere of core radius $r_{cx} = 0.6$ Mpc, the mean value of the major and minor axes. Either an oblate or a prolate spheroid with major and minor axes of 0.8 Mpc and 0.42 Mpc would change the density estimate by less than 20%. For the parameters of the X-ray coronae we have computed the average area using all those X-ray clumps associated with galaxies, from which we then computed a characteristic radius of 0.′72 [$26(H_0/50)^{-1}$ kpc] assuming spherical symmetry. A typical luminosity was chosen as 5×10^{41} ergs s^{-1} (see Table 4). The density and mass of the galactic coronae in Table 6 were computed assuming that the emission is due to an isothermal gas sphere with an assumed temperature of 1.2×10^7 K (= 1.0 keV). The Gaunt factor of an optically thin hot plasma in the 0.5–3 keV range varies weakly with temperature between 0.5×10^7 K and 3.0×10^7 K, so the density estimate is not sensitive to temperature.

c) Environmental Effects of the Cluster Gas

It is difficult to maintain the X-ray coronae in the face of ram pressure stripping and evaporation for galaxies of mass $3 \times 10^{11}\ M_\odot$ moving with velocities $v \approx \sigma_v$ through the cluster core. We have estimated several time scales and mass loss rates for the hot coronae. The evaporation rates were computed with the formulae given by Cowie and McKee (1977). The ram pressure stripping time scale is approximated by

$$t_{ST} \sim (R/v_g)(32n_c/9n_{cl})^{1/2} ,$$

where v_g is the velocity of the galaxies (1408 km s^{-1} [Danese, DeZotti, and diTullio 1980]), n_c is the number density of electrons in the galactic corona, n_{cl} is the number density of electrons in the cluster core, and R is the radius of the galactic corona (Gisler 1976; Lea and DeYoung 1976; Gunn and Gott 1972).

At the cluster center, the mass loss rates from ram pressure stripping and thermal evaporation are 135 $M_\odot$ yr^{-1} and 53 $M_\odot$ yr^{-1}, respectively. Varying the assumptions made in § III*b* within reasonable limits changes these estimates by at most a factor of 2. Mass loss from stars in the underlying galaxies cannot sustain the coronae since the maximum gas replenishment rate for a galaxy of $10^{12}\ M_\odot$ is 10 $M_\odot$ yr^{-1} (Faber and Gallagher 1976; Gisler 1979; Coleman and Worden 1976).

We have considered alternatives for maintaining the coronae.

i) If the galaxies with coronae have low velocities with respect to the cluster mean, then the effects of ram pressure will be reduced. Two of the galaxies with coronae in fact have radial velocities with respect

TABLE 6

GAS PARAMETERS OF A1367

Parameter	Galactic Corona	Cluster Core	Cluster Outskirts ($=3r_{cx}$)
Luminosity (ergs s^{-1})	5×10^{41}	4×10^{43}	...
Temperature (K)	1.2×10^7	3×10^7	3×10^7
Density (cm^{-3})	1.2×10^{-2}	7×10^{-4}	2×10^{-5}
X-ray core radius (kpc)	26	600	...
Gas mass ($M_\odot$)	2×10^{10}	1×10^{13}	...
Electron mean free path (kpc)	...	6	100

to the cluster mean that are less than 50 km s^{-1}. However, the velocity dispersion of all those galaxies with coronae is not significantly different from the velocity dispersion of those galaxies without coronae, and some of the galaxies with coronae have large (1500 km s^{-1}) velocities with respect to the mean.

ii) Massive dark halos can bind the gas in the face of both ram pressure stripping and evaporation. If the galaxies with coronae have sufficiently large masses such that (Mathews and Baker 1971)

$$GM/R > \tfrac{3}{2}kT/m_{\rm H} ,$$

then ram pressure stripping, except for high-velocity galaxies, will be ineffective. Though evaporation may heat up the gas to the ambient cluster temperature, the gas will not escape from the galaxy. The masses implied for these halos are $\sim 4 \times 10^{12}(kT/3$ keV$)(H_0/50)^{-1}\ M_\odot$ within $26(H_0/50)^{-1}$ kpc, which are larger than masses inferred for most galaxies (Faber and Gallagher 1979). Since the existence of a detectable corona is not correlated with high optical luminosity, it is unlikely that massive halos bind the coronae.

iii) If the galaxies with coronae do not reside in the core, but are presently in regions of lower density, the importance of conduction and ram pressure stripping would be decreased. Galaxies of mass $3 \times 10^{11}\ M_\odot$ will prevent ram pressure stripping of their X-ray coronae if they lie more than one core radius from the cluster center, and the mass loss rate from evaporation will be reduced to about $19\ M_\odot\ {\rm yr}^{-1}$.

iv) Further reductions in the evaporation loss rates could come about from magnetic fields in the galaxy, which would reduce the efficiency of conduction (Binney and Cowie 1981).

In sum, a galaxy can have a corona if (1) it resides in the core but is slow moving and has a massive halo or large magnetic field, or (2) it lives outside the central region and is only seen in projection on the cluster core. In this second picture the galaxies with coronae may be those that have only recently turned around from the initial Hubble expansion and are approaching the cluster center for the first time (Fabian, Schwarz, and Forman 1980).

Three galaxies (18, 35, and 33) with X-ray coronae have been observed at 21 cm, and all have been found deficient in neutral hydrogen, with $\log (M_{\rm H}/M_\odot) \leq 8.8$ (Table 5). This suggests that the cool disk gas in these galaxies has been heated to X-ray temperatures and is being swept or evaporated away.

Norman and Silk (1979) have argued that most of the present intergalactic medium in clusters can be accounted for by the liberation of halo gas from galaxies at a late epoch through collisions and ram pressure stripping. We find, however, that the amount of intracluster gas we observe in A1367 is somewhat larger than can easily be accounted for by the gas being removed from the galaxies today (Table 6). If each galaxy contributes $2 \times 10^{10}\ M_\odot$ in gas, then 500 galaxies are required to produce the observed intracluster gas. The implication is that some of the intracluster medium has never been processed through galaxies and is of primordial origin (Tinsley and Larson 1979).

d) Comparison with Other Observations

We expect other dynamically young clusters to have coronae as long as the ambient cluster gas temperature, the intracluster gas density, and the random velocity of the galaxies are comparable to those of A1367. The only other young cluster studied with comparable sensitivity and spatial resolution is Virgo. Forman *et al.* (1979) surveyed six Virgo galaxies with the *Einstein Observatory* within about 0.5 Mpc of M87, but outside the inner 0.25 Mpc, where M87 is dominant (Fabricant, Lecar, and Gorenstein 1980). Here, the density gas is about $5 \times 10^{-4}(H_0/50)^{1/2}$, and thus conditions are similar to those in the core of A1367. Forman *et al.* (1979) found one galaxy in their sample, M86, with an associated X-ray source of large enough extent to have been resolved by the HRI at the distance of A1367. They measured an X-ray luminosity of 2×10^{41} ergs s^{-1} (0.5–3.0 keV) and a core radius of 20 kpc for this source. At the distance of A1367, the asymmetry of the M86 source would appear only as a displacement of the centroid of the X-ray emission from the center of the optical galaxy by about 25″. In A1367 we find displacements of the extended sources from their associated galaxies of up to 28″. Since, however, we estimate the 90% error radius for the X-ray centroids to be about 15″ due to systematic and statistical errors, these displacements are consistent with a random distribution and therefore we cannot measure an intrinsic 25″ displacement. Thus, although limited to one, the observations of a galactic corona in Virgo are consistent in luminosity, and size with those observed in A1367.

In relaxed clusters such as Coma, we would not expect to find coronae. If galactic halos existed in early stages, they would have been stripped by tidal interactions between galaxies. The high density, high temperature, and the broad distribution of the ambient gas, make evaporation and ram pressure stripping more effective in removing coronae in Coma-type systems.

Little information is available concerning hot coronae around field galaxies. Feigelson *et al.* (1981) reported a possible diffuse component of about 3×10^{40} ergs s^{-1} in Centaurus A (NGC 5128) which could be interpreted as a galactic wind (Mathews and Baker 1971), although other explanations are plausible. In M31 all the X-ray flux observed by *Uhuru* can be accounted for by point sources (Van Speybroeck *et al.* 1979), and the X-ray luminosity of a corona is limited to $L_x < 1 \times 10^{39}$ ergs s^{-1}.

e) 1′ Sources with No Associated Cluster Galaxy

The nature of the extended HRI sources with no apparent cluster galaxy is uncertain. On the one hand, their apparent X-ray fluxes and extents are consistent with their being Coma type or cD clusters at $z = 0.5$–1.0, so that optically they would be difficult to detect. On the other hand, the X-ray luminosity functions for clusters given by Bahcall (1979), Piccinotti *et al.* (1982), or McKee *et al.* (1980) predict that approximately 0.1 clusters per

HRI field should be observed at the flux limit of H6062, assuming no evolution and $q_0 = 0$. In the *Einstein* Medium Sensitivity Survey, Maccacaro *et al.* (1982) find clusters in numbers that are consistent with this prediction. In H6062, however, three extended sources are observed, which are not associated with any cluster galaxy. It is unlikely that these are spurious, since although the detection thresholds are set to allow at most one spurious source per field, these three sources are well above threshold, and in fact brighter than most sources associated with cluster galaxies. Even if one is spurious, the probability of seeing two clusters when 0.1 is expected is 4.5×10^{-3}. Evolutionary and cosmological effects probably lower the number of clusters expected (Perrenod 1978; Schwartz 1976). Although the probability of finding three clusters from a uniformly distributed population is small, a plausible explanation is that we have observed a supercluster behind A1367. The spatial covariance function for Abell clusters indicates that the probability of finding a cluster within 40 Mpc of a given cluster is 10 times the probability calculated from a random distribution of clusters (Hauser and Peebles 1973). At a redshift of ~ 0.4 (based on the magnitudes of the brightest galaxies) the cluster separations would be ~ 5 Mpc, a typical supercluster scale (Karachentsev, Tsarevskaya, and Scherbanovskii 1976; Hauser and Peebles 1973). If, instead, these sources are associated with A1367, their survival in the face of evaporation by the ambient medium is difficult to understand.

VI. CONCLUSIONS

We have observed X-ray coronae associated with eight galaxies in A1367. In the context of the dynamical evolution of clusters, these galaxies may represent material that has only recently turned around from the Hubble flow and which has not yet virialized with the inner portions of the cluster. This hypothesis should be testable in other clusters with similar morphologies.

We thank W. Ku for allowing us to use the HRI images of Coma. We are grateful to G. Bothun, G. Chincarini, J. Stauffer, and W. Tifft for use of their data prior to publication, A. Oemler for his list of galaxy counts, and S. Strom and K. Strom for prints of their 4 meter plates. M. Fener helped prepare the figures. Finally, we thank Y. Avni, M. Geller, and S. Kent for helpful discussions, and K. Gilleece for preparing the manuscript. This work was sponsored under NASA contract NAS8-30751.

REFERENCES

Bahcall, N. 1977, *Ap. J.* (*Letters*), **218**, L93.
———. 1979, *Ap. J.* (*Letters*), **232**, L83.
Bechtold, J., *et al.* 1983, in preparation.
Binney, J., and Cowie, L. L. 1981, *Ap. J.*, **247**, 464.
Carter, D., and Metcalf, N. 1980, *M.N.R.A.S.*, **191**, 325.
Chincarini, G., Giovanelli, R., Haynes, M., and Fontanelli, P. 1982, preprint.
Coleman, G. D., and Worden, S. P. 1976, *Ap. J.*, **205**, 475.
Cowie, L. L., and McKee, C. F. 1977, *Ap. J.*, **211**, 135.
Danese, L., DeZotti, G., and diTullio, G. 1980, *Astr. Ap.*, **82**, 322.
Elvis, M., Schreier, E. J., Tonry, J., Davis, M., and Huchra, J. P. 1981, *Ap. J.*, **246**, 20.
Faber, S. M., and Gallagher, J. S. 1976, *Ap. J.*, **204**, 365.
Fabian, A. C., Schwarz, J., and Forman, W. 1980, *M.N.R.A.S.*, **192**, 135.
Fabricant, D., Lecar, M., and Gorenstein, P. 1980, *Ap. J.*, **241**, 552.
Feigelson, E. D., Schreier, E. J., Delvaille, J. P., Giacconi, R., Grindlay, J. E., and Lightman, A. P. 1981, *Ap. J.*, **251**, 31.
Forman, W., Kellogg, E., Gursky, H., Tanabaum, H., and Giacconi, R. 1972, *Ap. J.*, **178**, 309.
Forman, W., Schwarz, J., Jones, C., Liller, W., and Fabian, A. C. 1979, *Ap. J.* (*Letters*), **234**, L27.
Gavazzi, G. 1978, *Astr. Ap.*, **69**, 355.
Giacconi, R., *et al.* 1979*a*, *Ap. J.*, **230**, 540.
Giacconi, R., *et al.* 1979*b*, *Ap. J.* (*Letters*), **234**, L1.
Gisler, G. 1976, *Astr. Ap.*, **51**, 137.
———. 1979, *Ap. J.*, **228**, 385.
Griffiths, R. E., *et al.* 1982, *Ap. J.*, submitted.
Gunn, J., and Gott, R. 1972, *Ap. J.*, **176**, 1.
Gursky, H., Kellogg, E., Leong, C., Tananbaum, H., and Giacconi, R. 1971, *Ap. J.* (*Letters*), **167**, L81.
Hauser, M. G., and Peebles, P. J. E. 1973, *Ap. J.*, **185**, 757.
Jones, C., Mandel, E., Schwarz, J., Forman, W., Murray, S. S., and Harnden, F. R., Jr. 1979, *Ap. J.* (*Letters*), **234**, L21.
Karachentsev, I. D., Tsarevskaya, R. L., and Scherbanovskii, A. L. 1976, *Soviet Astr.*, **19**, 606.
Kellogg, E., Tananbaum, H., Giacconi, R., and Pounds, K. 1972, *Ap. J.* (*Letters*), **174**, L65.
Ku, W. 1981, private communication.
Lea, S. M., and DeYoung, D. S. 1976, *Ap. J.*, **210**, 647.
Long, K., and Van Speybroeck, L. P. 1982, in *Accretion Driven Stellar X-Ray Sources*, ed. W. Lewin (in press).
Maccacaro, T., *et al.* 1982, *Ap. J.*, **253**, 504.
Mathews, W. G., and Baker, J. C. 1971, *Ap. J.*, **170**, 241.
McKee, J., Mushotzky, R., Boldt, E., Holt, S., Marshall, F. E., Pravdo, S., and Serlemitsos, P. 1980, *Ap. J.*, **242**, 843.
Mushotzky, R. F., Serlemitsos, P. J., Smith, B. W., Boldt, E. A., and Holt, S. S. 1978, *Ap. J.*, **225**, 21.
Norman, C., and Silk, J. 1979, *Ap. J.* (*Letters*), **233**, L1.
Oemler, A. 1980, private communication.
Perrenod, S. C. 1978, *Ap. J.*, **226**, 566.
Piccinotti, G., Mushotzky, R. F., Boldt, E. A., Holt, S. S., Marshall, F. E., Serlemitsos, P. J., and Shafer, R. A. 1982, *Ap. J.*, **253**, 485.
Raymond, J. C., Cox, D. P., and Smith, B. W. 1976, *Ap. J.*, **204**, 290.
Rees, M., and Ostriker, J. P. 1977, *M.N.R.A.S.*, **179**, 541.
Schwartz, D. A. 1976, *Ap. J.* (*Letters*), **206**, L95.
Strom, K. M., and Strom, S. E. 1978*a*, *A.J.*, **83**, 73.
Strom, S. E., and Strom, K. M. 1978*b*, *A.J.*, **83**, 732.
Sullivan, W., and Johnson, P. 1978, *Ap. J.*, **225**, 751.
Tifft, W. G. 1978, *Ap. J.*, **222**, 54.
Tinsley, B. M., and Larson, R. B. 1979, *M.N.R.A.S.*, **186**, 503.
Van Speybroeck, L., Epstein, A., Forman, W., Giacconi, R., Jones, C., Liller, W., and Smarr, L. 1979, *Ap. J.* (*Letters*), **234**, L45.
White, S. D. M. 1976, *M.N.R.A.S.*, **177**, 717.

J. BECHTOLD: Steward Observatory, University of Arizona, Tucson, AZ 85721

W. FORMAN, C. JONES, J. SCHWARZ, W. TUCKER, and L. VAN SPEYBROECK: Harvard-Smithsonian Center for Astrophysics, 60 Garden Street, Cambridge, MA 02139

R. GIACCONI: Space Telescope Science Institute, Homewood Campus, Baltimore, MD 21218

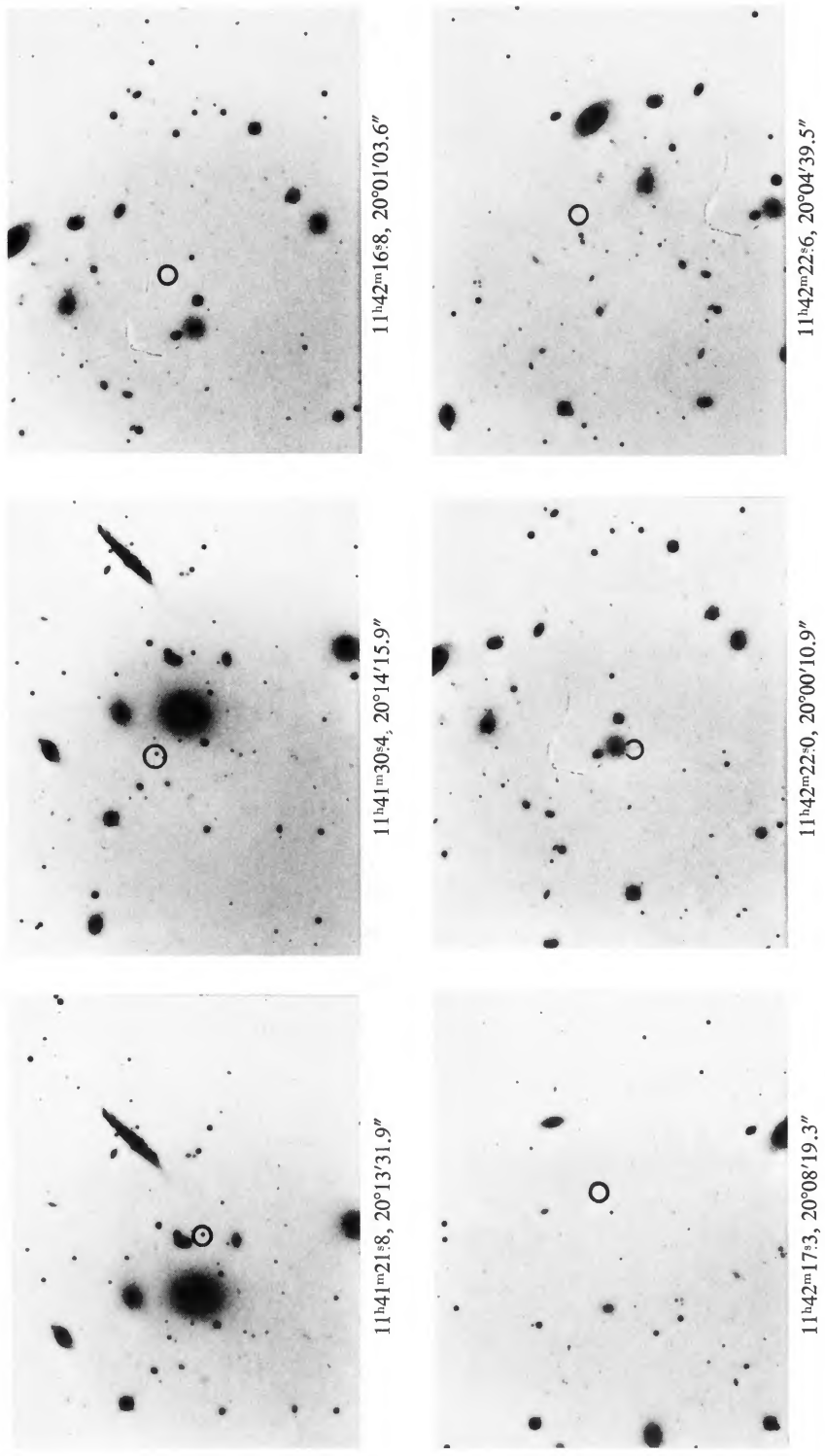

FIG. 1.—Finding charts for point sources in A1367 as listed in Table 2. Circles correspond to 90% confidence contours drawn on a blue 4 m plate of Strom and Strom (private communication). North is up and east is to the left.

PLATE 2

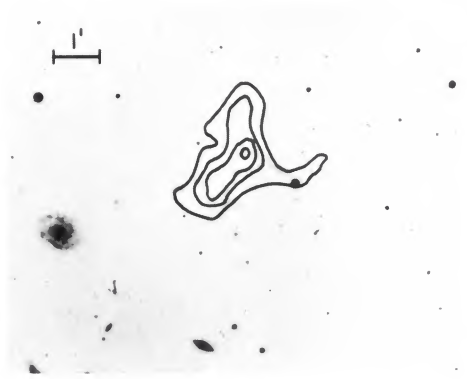

$11^h41^m08^s.3$, 20°22′11″.7

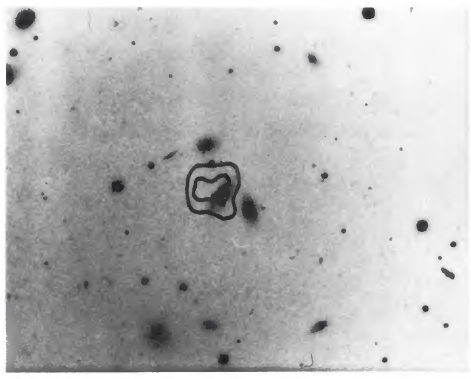

$11^h41^m27^s.7$, 20°03′42″.8

$11^h41^m29^s.2$, 20°17′34″.4

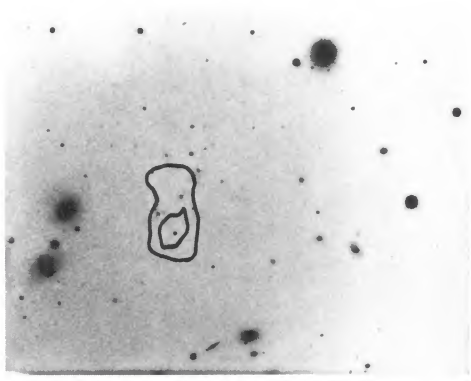

$11^h41^m33^s.9$, 20°07′03″.7

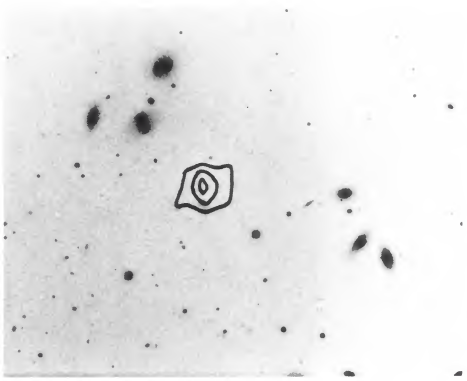

$11^h41^m37^s.3$, 20°04′42″.9

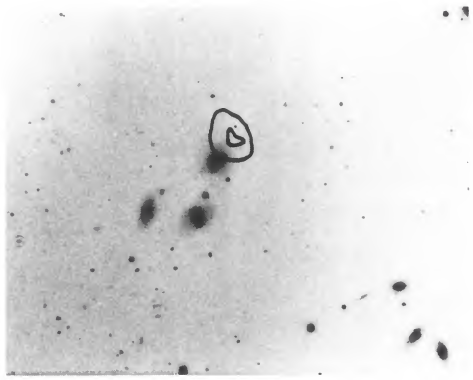

$11^h41^m42^s.0$, 20°06′48″.8

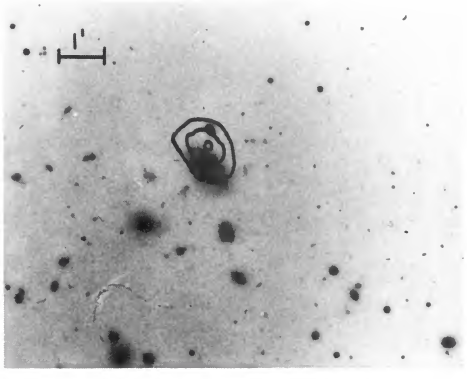

$11^h42^m13^s.0$, 20°04′42″.6

FIG. 2.—Finding charts for extended 1′ sources in A1367 as listed in Table 4. Isointensity contours represent 2 σ, 3 σ, 4 σ, and 5 σ above local background, and are drawn on a blue 4 m plate of Strom and Strom (private communication). North is up and east is to the left.

BECHTOLD *et al.* (*see* page 28)

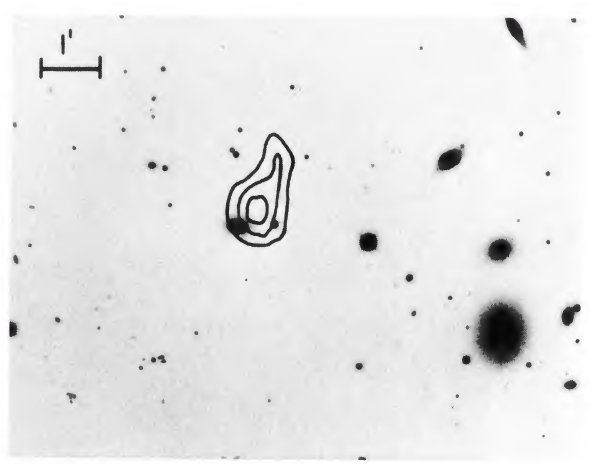

$11^h41^m44^s.1$, 20°15′43″.9

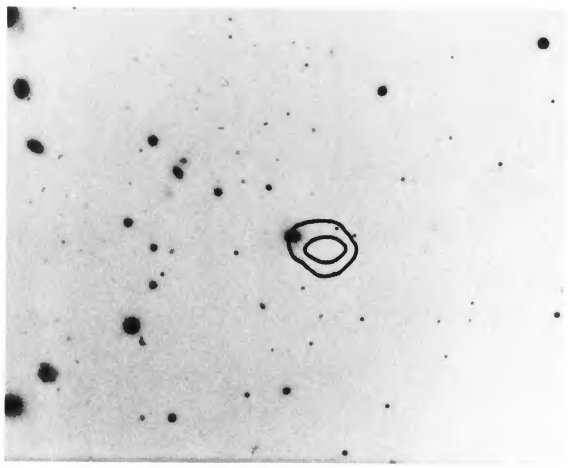

$11^h41^m51^s.8$, 20°00′27″.2

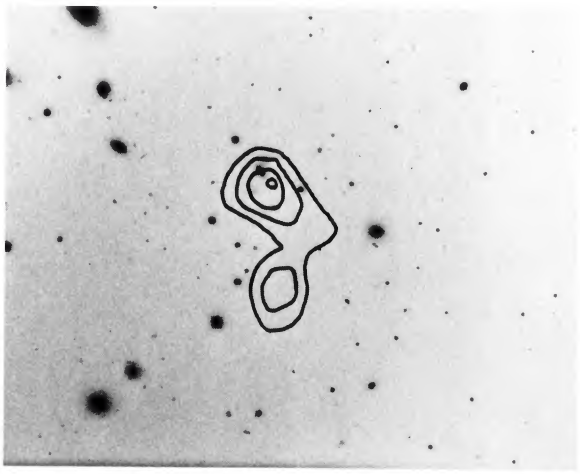

$11^h42^m01^s.0$, 20°01′22″.2

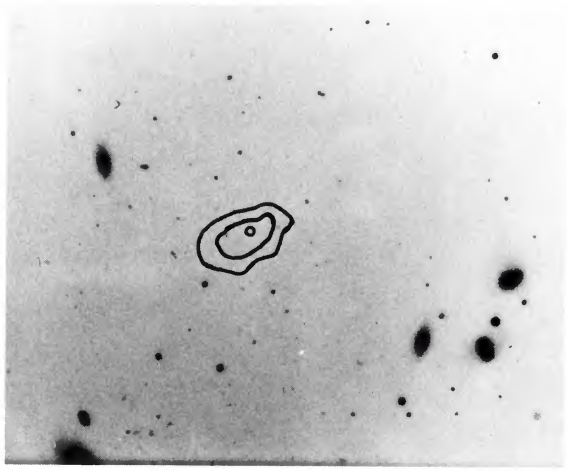

$11^h42^m01^s.6$, 20°08′20″.0

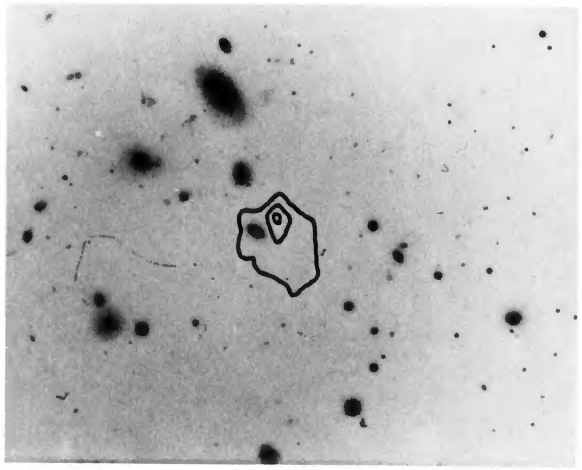

$11^h42^m10^s.2$, 20°02′05″.5

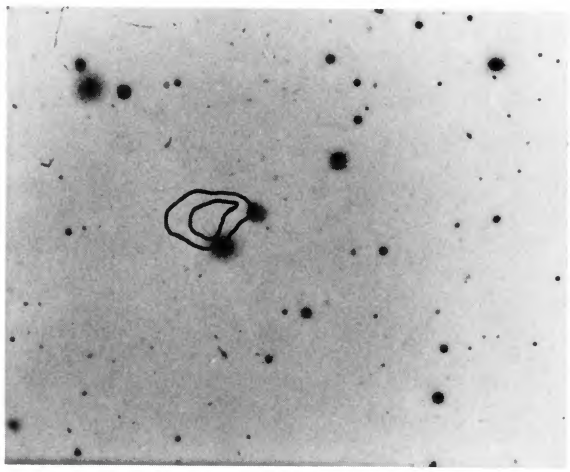

$11^h42^m12^s.8$, 19°58′15″.0

FIG. 2.—*Continued*

PLATE 4

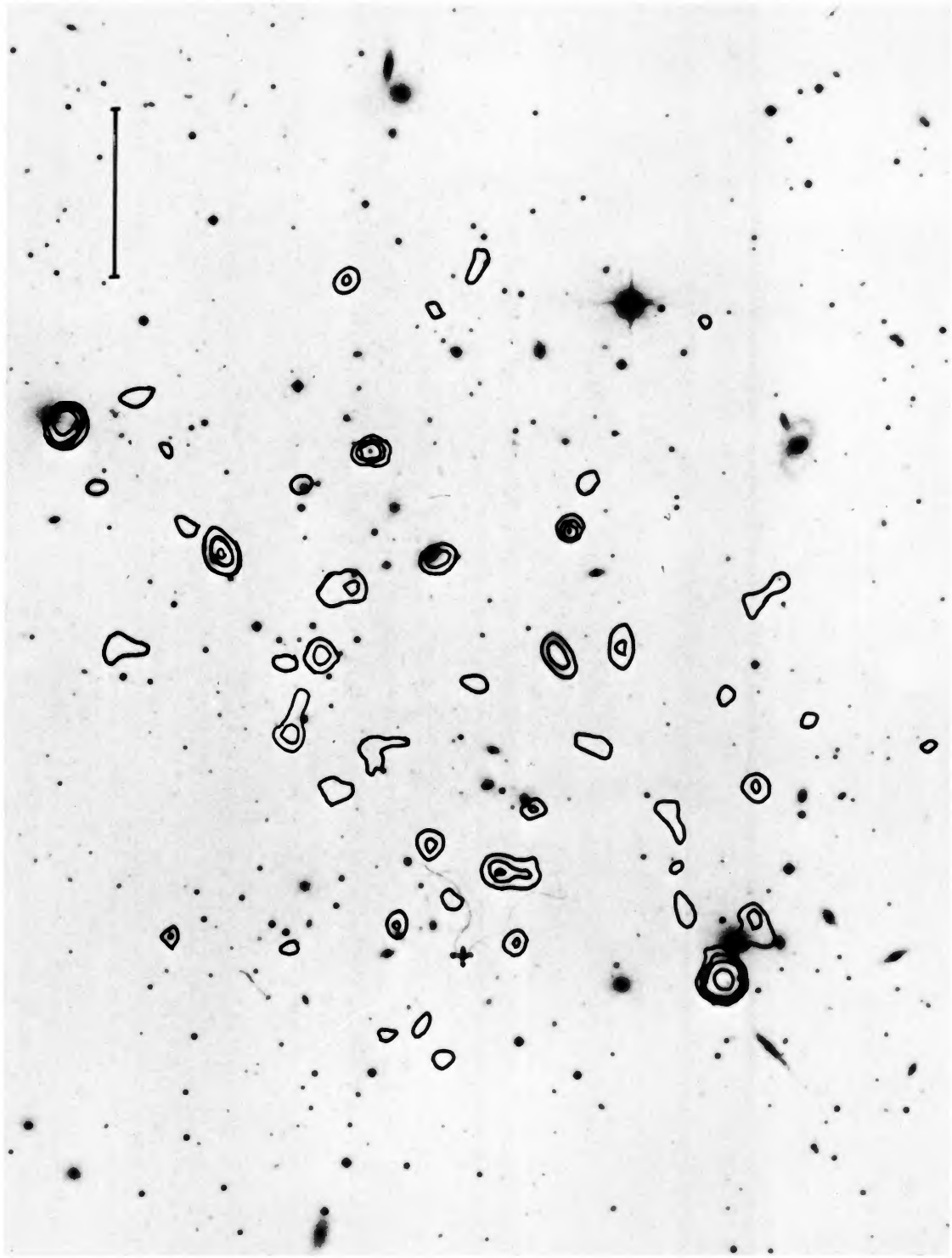

FIG. 3.—HRI isointensity contours superposed on red Palomar Sky Survey print. The larger scale diffuse cluster emission has been subtracted. Contour levels represent 2 σ, 3 σ, 4 σ, and 5 σ above local background. North is up and east is to the left. The X-ray emission associated with the galaxy NGC 3862 appears displaced because of its location at the extreme edge (south-east) of the detector. The length of the bar at the lower left of the figure is 5′.

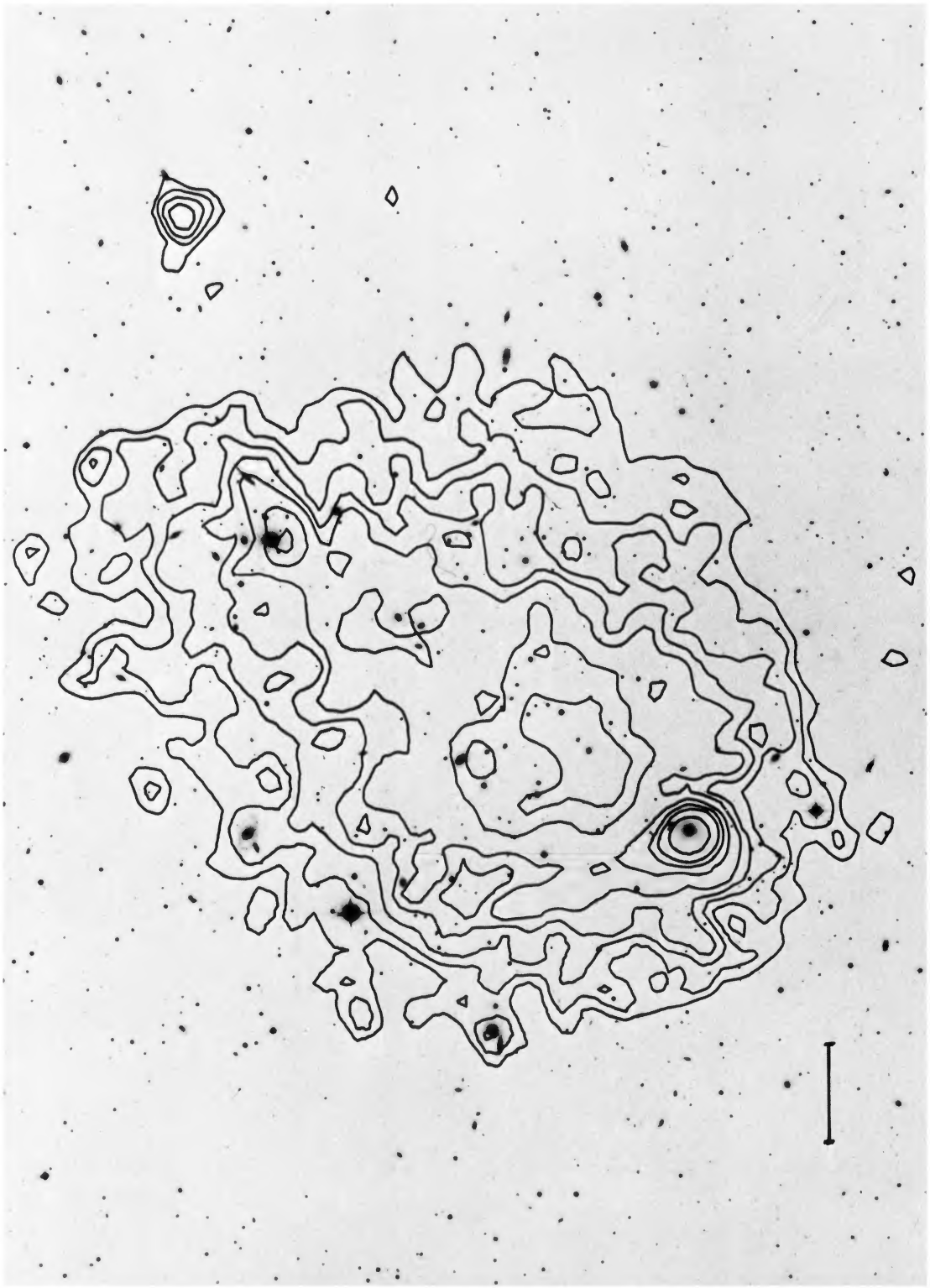

FIG. 4.—IPC isointensity contours for 0.5 to 3 keV band superposed on red Palomar Sky Survey print. The X-ray contours have been generated by smoothing the data with a 32″ Gaussian, subtracting noncluster background and plotting 3 σ, 5 σ, 7 σ, 9 σ, and 11 σ confidence levels. North is up and east is to the left. The length of the bar at the lower left of the figure is 5′.

BECHTOLD *et al.* (*see* page 29)